Journal of the European Ceramic Society **15** (1995) 329–335
1995 Elsevier Science Limited
Printed in Great Britain
0955-2219/95/$9.50

Corrosion Resistance of Ceramic-coated Stainless Steel in a Br_2–O_2–Ar Atmosphere

Makoto Sasaki & Toshio Hirai

Institute for Materials Research, Tohoku University, Katahira 2-1-1, Aoba-ku, Sendai 980, Japan

(Received 13 May 1994; revised version received 15 July 1994; accepted 12 August 1994)

Abstract

Coatings of SiC/TiC compositional graded film (FGM), m-HfO_2 and c-HfO_2 films on stainless steel (SUS304) plates have been investigated as candidate materials for 'UT-3' which is an effective process of hydrogen production through thermochemical decomposition of water. Changing the source gas concentration leads to composition control in TiC–SiC composite films. Cracks in the films could not be avoided in either the TiC-coated SUS304 nor the SiC–TiC double layer-coated SUS304. However the SiC/TiC FGM-coated SUS304 had no cracks. Corrosion of the TiC and SiC–20 mol%TiC double-layer-coated SUS304 in the Br_2–O_2–Ar atmosphere was mainly caused by oxidation of the TiC film and SUS304. The SiC/TiC FGM-coated SUS304 showed superior corrosion resistance in isothermal and cyclic heating conditions.

m-HfO_2 and c-HfO_2 (7·1–44·5 mol% Y_2O_3) were attained by the changing of $Y(DPM)_3$ gas concentration. XRD measurement shows the monoclinic and cubic HfO_2. Both plate-like and columnar texture in the m-HfO_2 and c-HfO_2 films were observed. m-HfO_2, in which columnar texture, coated SUS304 showed the excellent corrosion resistance in Br_2–O_2–Ar atmosphere under heat cyclic conditions. This is thought to be due to the effects of columnar texture on the thermal stress relaxation, and of the excellent corrosion resistance of the m-HfO_2.

1 Introduction

Hydrogen gas (H_2) is expected to be used as a new energy source because conventional fuels tend to destroy the natural environment. One of the methods to produce H_2 is the thermochemical decomposition of water called 'UT-3'.[1] The 'UT-3' process causes high temperature corrosion of structural materials because highly corrosive gases such as O_2, Br_2 and HBr might be used at temperatures from 500 to 1000 K. Considering practical applications, metals should be used as structural materials. However, no metal is known to resist the corrosive conditions caused by 'UT-3'. Ceramic-coated metals are expected to be candidate structural materials. Titanium carbide (TiC) films are highly adherent to metals, and silicon carbide (SiC) is resistant to corrosion. CVD is the most suitable method for the surface modification of metals, because it allows the preparation of dense and adherent films. On the other hand, Functionally Gradient Materials (FGMs) having an excellent thermal stress relaxation property are well known as thermal barrier materials.[2–7] In the present work, single-layer TiC or SiC, double-layer SiC and TiC, and SiC/TiC FGM coatings were placed on stainless steel (SUS304) using the CVD method. On the other hand, HfO_2 has a superior thermal expansion matching to the stainless steel. Thus, m-HfO_2 and c-HfO_2(Y_2O_3) coatings were also deposited on the SUS304 using the CVD method. The corrosion behaviour of these materials in Br_2–O_2–Ar atmosphere was investigated.

2 Experimental

2.1 Preparation of TiC, SiC and SiC–TiC composite films

Stainless steel (SUS304) plates (15 mm in diameter and 2 mm in thickness) were used as substrates. Source gases $TiCl_4$, CH_3SiCl_3(MTS), CH_4 and H_2 were introduced into a hot-wall type CVD reactor. Deposition temperature (T_{dep}) and total gas pressure (P_{tot}) were fixed at 1323 K and 0·1 MPa, respectively. H_2 gas flow rate was kept at $8{\cdot}3 \times 10^{-6}m^3s^{-1}$. $TiCl_4$ gas flow rate was changed from 0 to $3{\cdot}3 \times 10^{-7}m^3s^{-1}$, MTS gas flow rate from 0 to $1{\cdot}6 \times 10^{-6}m^3s^{-1}$. The ratio of CH_4 to MTS was kept at 1·7 to fabricate the TiC-containing films. The structure of CVD films was examined by XRD (Rigaku: RAD-C), the surface and the

Table 1. Preparation conditions of m-HfO_2

Substrate temperature (T_{sub}), T/K	873~1173
Total gas pressure (P_{tot}), P/kPa	1·3
Gas flow rate, $FR/10^{-6}m^3s^{-1}$	
Ar for $Hf(DPM)_4$	1·7
O_2	1·7
Temperature of $Hf(DPM)_4$ reservoir (THf), T/K	453
Deposition time (T_{dep}), t/ks	1·2~4·8

Table 2. Preparation conditions of c-HfO_2

Substrate temperature (T_{sub}), T/K	873~1073
Total gas pressure (P_{tot}), P/kPa	1·3
Gas flow rate, $FR/10^{-6}m^3s^{-1}$	
Ar for $Hf(DPM)_4$	1·7
Ar for $Y(DPM)_3$	1·7
O_2	1·7
Temperature of $Hf(DPM)_4$ reservoir (THf), T/K	433~463
$Y(DPM)_3$ reservoir (THf), T/K	403~421
Deposition time (T_{dep}), t/ks	1·2~7·2

cross-sectional texture observed by SEM spectroscopy (Akashi:ALPHA-30). SiC and TiC content in the films were determined by EPMA measurement as substitutions for the Si (Ka) and Ti (Ka) intensity.

2.2 Preparation of SiC/TiC FGM film

On the basis of the preparation conditions of SiC–TiC composite films, SiC/TiC FGM films were fabricated on SUS304 by changing the source gas concentration ('a'=MTS/($TiCl_4$+MTS)) at T_{dep}=1323 K and P_{tot}=0·1 MPa. 'a' was changed stepwise from 0 for 4 h, 0·7 for 1 h to 1·0 for 1 h. The surface and cross-sectional texture were observed by SEM.

2.3 Preparation of m- and c-HfO_2 films

(100)Si and Stainless steel (SUS304) plates (15 mm in diameter and 2 mm in thickness) were used as substrates. Source gases $Hf(DPM)_4$, $Y(DPM)_3$, O_2 and Ar were introduced into a hot-wall type CVD reactor. Tables 1 and 2 demonstrate the CVD conditions. Deposition temperature (T_{dep}) and total gas pressure (P_{tot}) were fixed at 1073 K and 13 kPa, respectively. The structure of CVD films was examined by the XRD, the surface and the cross-sectional texture observed by the SEM. Film composition was determined by ICP and XRF measurements.

2.4 Measurement of corrosion rates

Figure 1 demonstrates the experimental set-up for the evaluation of corrosion rate. The specimens were suspended by a platinum wire in an electric furnace. Weight changes during corrosion were continuously measured using an electric balance connected to a computer (NEC:PC-9801). The electric balance was kept at 298 K in a constant temperature box. Ar gas was passed through the electric balance and introduced into the quartz tube. O_2 gas containing Br_2 was introduced from the bottom of the balance box into the quartz tube. The Br_2 reservoir was maintained at 288 K. The corrosion temperature (T_{cor}) was kept at 1173 K in isothermal experiments. In the case of cyclic heating, T_{cor} was cyclically changed from 1173 to 773 K under the same gas flow rates in isothermal corrosion experiment.

3 Results and discussion

3.1 Preparation of TiC, SiC and SiC–TiC composite films

The possibility of the CVD method to control film composition was investigated. Figure 2 shows the relationship between input gas concentration and film composition. SiC content in the film increases

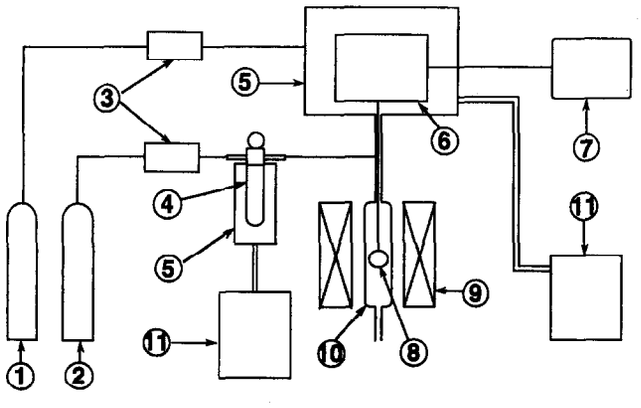

Fig. 1. Schematic diagram of corrosion rate measurement: (1) Ar gas, (2) O_2 gas, (3) mass flow meter, (4) Br_2 reservoir, (5) constant temperature bath, (6) electric balance, (7) computer, (8) specimen, (9) electric furnace, (10) quartz tube, (11) cool pump.

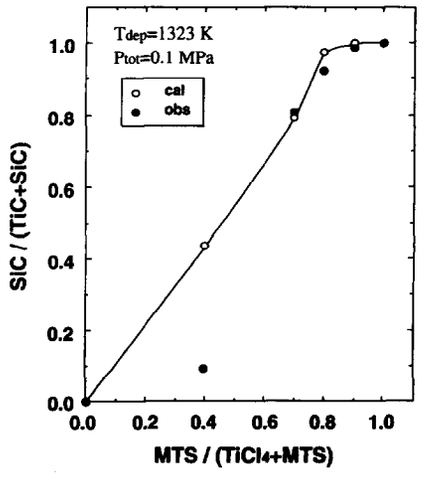

Fig. 2. Relationship between input gas concentration and film composition compared with theoretical film composition.

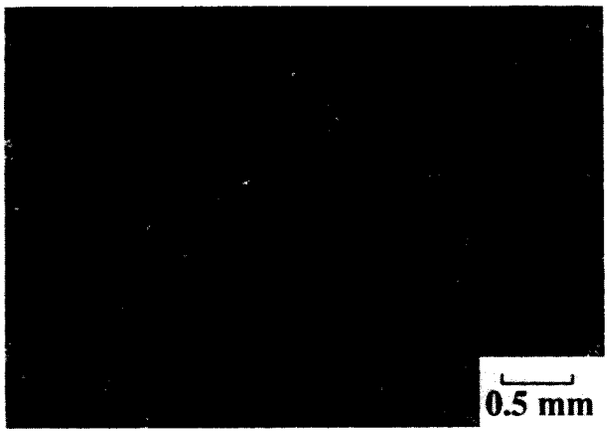

Fig. 3. SEM photograph of deposited surface of the SiC and TiC double-layer-coated SUS304.

with increasing MTS concentration. Figure 2 also demonstrates the theoretical composition of the films calculated using JANAF data[8] under the thermodynamic equilibrium conditions based on a free energy minimisation method. Experimental compositions of the films agree well with those of the calculated values except at the *a* of 0·4. The lower value is thought to be due to the kinetics of the CVD process. These data show that SiC content in the SiC–TiC composite films can be controlled.

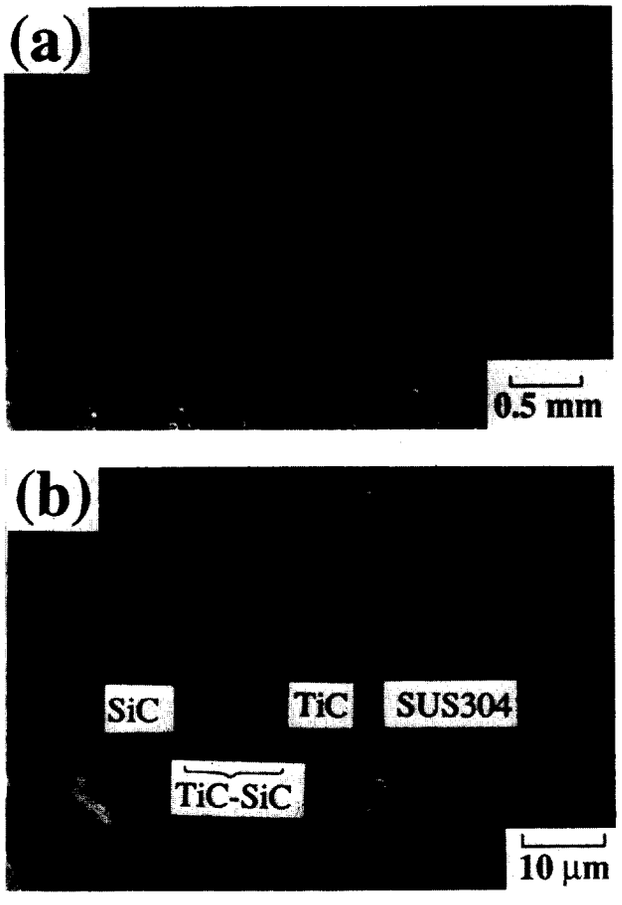

Fig. 4. SEM photographs of the SiC/TiC FGM-coated SUS304. (a) Surface of the specimen. (b) Cross-section of the specimen.

While direct coating of TiC on the SUS304 was achieved, the SiC–TiC composite film was not obtained on the SUS304 because Fe_3Si and $FeSi_2$ formed as a result of easy reaction between MTS and SUS304. This result demonstrates the impossibility of direct coating of SUS304 with SiC. Reaction protection layers such as TiC are indispensable between SiC and SUS304. An SiC coating on the TiC-coated SUS304 was attempted. Figure 3 shows the SEM photograph of the surface of the SiC/TiC double layer-coated SUS304. SiC was deposited on the TiC interlayer. Cracks were observed on the surface of the TiC-coated SUS304. Thermal expansion coefficients of TiC, SiC and SUS304 are $7{\cdot}6 \times 10^{-6}$, $4{\cdot}3 \times 10^{-6}$, $1{\cdot}73 \times 10^{-5}K^{-1}$, respectively. As shown in Fig. 4, cracking also occurred in the SiC film as a result of the mismatch between thermal expansion coefficients of SiC and SUS304. Even if the thicknesses of SiC and TiC were ranged from 2 to 20 μm, cracking could not be avoided.

3.2 Preparation of an SiC/TiC FGM film

For the purpose of residual thermal stress relaxation and the protection of crack formation, continuous change of the thermal expansion coefficients, so-called Functionally Gradient Materials (FGMs) might be useful. Figure 4 shows the SEM photographs of the surface and the cross-section of the SiC/TiC FGM-coated SUS304.

Compositional graded layer from TiC to SiC forms on the SUS304. Despite the mismatch of thermal expansion coefficients between SiC, TiC and SUS304, no cracks in the SiC/TiC FGM-coated SUS304 appear on the deposited surface, as shown in Fig. 4. The result suggests that the introduction of the compositional gradation between the SiC and TiC layers reduce the surface tensile stress of the SiC/TiC FGM-coated SUS304.

3.3 Synthesis of m-HfO_2 films

The m-HfO_2 formation was confirmed by X-ray diffraction (JCPDS card No. 34-104). The thickness increased from 0·8 to 3·2 μm with increasing T_{dep} from 873 to 1073 K, and was kept constant above 1073 K. The SEM photographs of the surface of m-HfO_2 deposited on the (100)Si substrate are shown in Fig. 5. Figure 5(a) shows a plate-like dense m-HfO_2 film deposited at a T_{dep} of 973 K and at a t_{dep} of 1·2 ks, which has cracks and detached from the substrate. On the other hand, as shown in Fig. 5(b), the film deposited at a T_{dep} of 1073 K and at a t_{dep} of 2·4 ks has a columnar texture. Figure 5(b) also shows the dense layer around the interface film-substrate with no cracks and no detachment from the substrate.

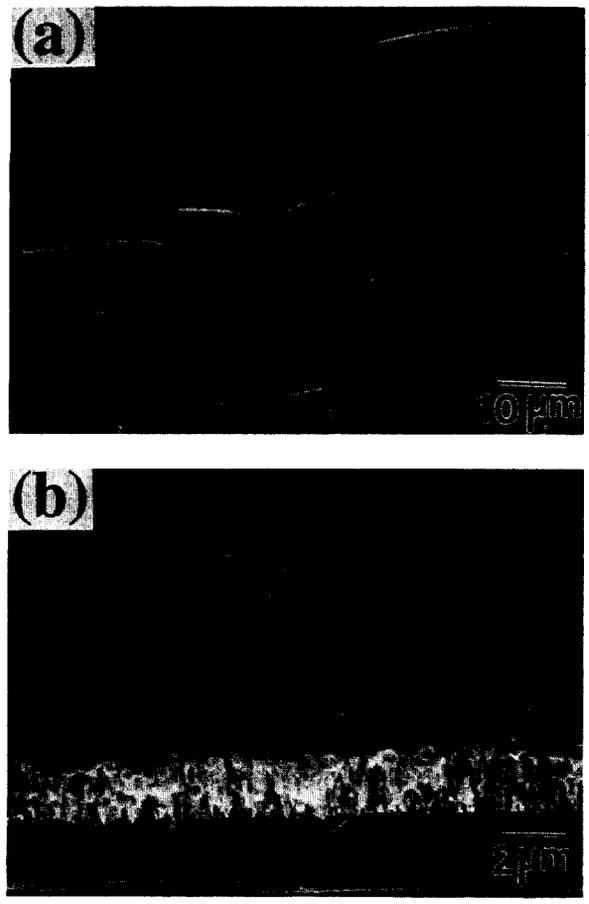

Fig. 5. SEM photographs of the plate-like (a) and columnar (b) m-HfO_2.

As shown in Fig. 5, a plate-like dense film was deposited in the T_{dep} range from 873 to 973 K. Its XRD pattern, characterised by broad peaks, demonstrated the lower degree of crystallisation. On the other hand, the film deposited in the T_{dep} range from 1023 to 1173 K has a columnar structure and showed relatively higher crystallinity.

3.4 Synthesis of c-HfO_2 films

The film deposited at a T_{dep} of 1073 K, a T_{Hf} of 453 K, a T_Y of 406 K, a t_{dep} of 2·4 ks, FA_{Ar} of 1·7 × 10^{-6} m^3s^{-1}, FR_{O_2} of 1·7 × 10^{-6} m^3s^{-1}, and at a P_{tot} of 1·3 kPa, was identified as the c-HfO_2 (JCPDS card No. 24-1406).

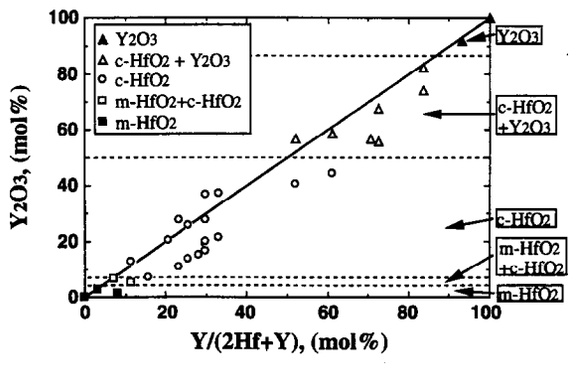

Fig. 6. Relationship between input gas concentration and film composition.

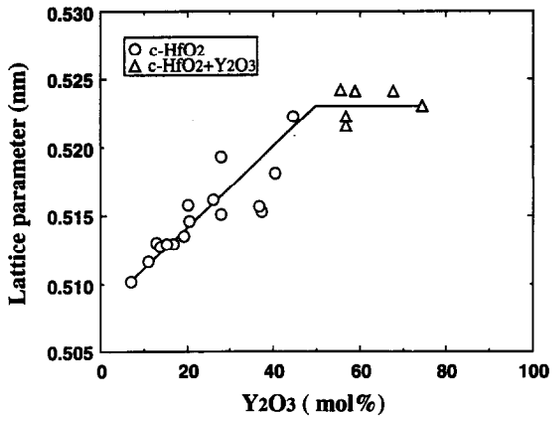

Fig. 7. Relationship between film composition and lattice parameter of c-HfO_2.

Figure 6 shows the relationship between input gas molar ratio and the Y_2O_3 content in the films. The straight line in Fig. 6 demonstrates the ideal Y_2O_3 content in the films, obtained by the following reaction:

$$x\mathrm{Hf(DPM)_4}+y\mathrm{Y(DPM)_3}+\mathrm{O_2}\rightarrow x\mathrm{HfO_2}+(y/2)\mathrm{Y_2O_3}+(\text{Volatile compounds})$$

Y_2O_3 content was determined by ICP method in which the substitution of Y content in the films. m-HfO_2+c-HfO_2) composites were deposited in the Y_2O_3 range from 5·03 to 6·52 mol%, single c-HfO_2 phase in the Y_2O_3 range from 7·1 to 44·5 mol%, c-HfO_2+Y_2O_3 composites in the Y_2O_3 range from 56·6 to 82·3 mol%.

The relationship between Y_2O_3 content and the lattice parameters measured by (400) X-ray intensity is shown in Fig. 7. The (400) peak of the substrate was used as an inner standard. The lattice parameters have a tendency to increase with increasing Y_2O_3 content.

3.5 Corrosion behaviour

(a) SiC–TiC composites and SiC/TiC FGM

Weight loss of the TiC-coated SUS304 during corrosion experiment was observed at T_{cor}=1173 K, P_{Br_2} = 4·4 kPa and P_{O_2} = 0·1 kPa. As large quantities of O_2 gas might be generated in the 'UT-3' process, corrosion experiments should be conducted at large O_2 gas concentration including Br_2 gas. Figure 8 shows the relationship between time and weight change by the corrosion at T_{cor}=1173 K, P_{Br_2} = 4·4 kPa and P_{O_2} = 46 kPa (isothermal corrosive condition). All the specimens revealed weight gain in this corrosive condition. The surfaces of the TiC-coated SUS304, TiC and SiC-20 mol% TiC double-layer-coated SUS304, and SiC and TiC double-layer-coated SUS304 after the corrosion at T_{cor}=1173 K, P_{Br_2} = 4·4 kPa and P_{O_2} = 46 kPa were observed by SEM. The surface of the TiC was extremely damaged by corrosion. In the case of the SiC-20 mol% TiC, the surface

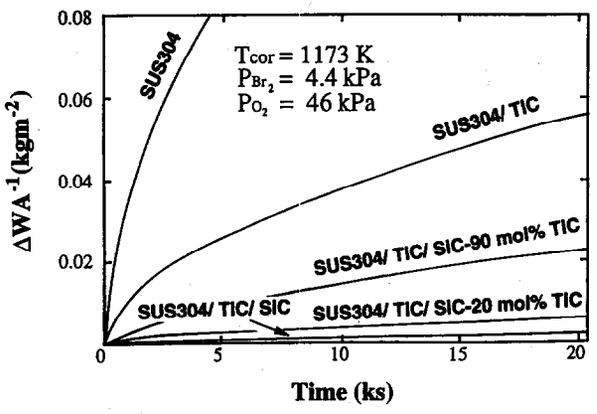

Fig. 8. Relationship between time and weight gain of the SiC–TiC composites by the corrosion at T_{cor} = 1173 K, P_{Br_2} = 4·4 kPa and P_{O_2} = 46 kPa.

texture became porous and rough. This result occurs due to the difference of corrosion rate between SiC and TiC. SiC is likely to have excellent corrosion resistance. Phases formed after corrosion were investigated by using XRD. TiO_2, Fe_2O_3 and Fe_3O_4 were observed at the surface of the TiC-coated SUS304. The SUS304 substrate was oxidised by corrosive Br_2–O_2 that diffused through the cracks of the TiC film. On the other hand, only TiO_2 was formed on the TiC/SiC-20 mol% TiC double-layer-coated SUS304.

Figure 9 shows the dependence of corrosion rate on the film composition in the SiC–TiC composite system. Clearly, the addition of SiC into the TiC film improves the corrosion resistance of TiC. SiC provide high corrosion resistance, but the TiC/SiC-20 mol% TiC can not be used as the surface material in 'UT-3', because a corrosion of TiC in the composite film is indispensable. To compare the corrosion resistance of TiC/SiC-20 mol% TiC double-layer-coated SUS304 with that of the SiC/TiC FGM-coated SUS304, a corrosion experiment with different heat cycles was attempted.

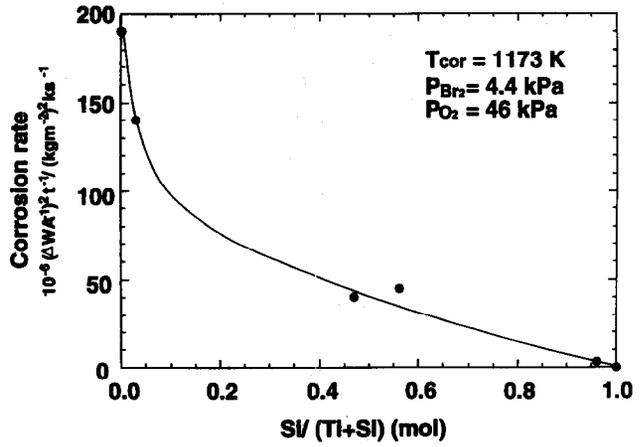

Fig. 9. Dependence of corrosion rate on the composition of SiC–TiC composite films by the corrosion at T_{cor} = 1173 K, P_{Br_2} = 4·4 kPa and P_{O_2} = 46 kPa.

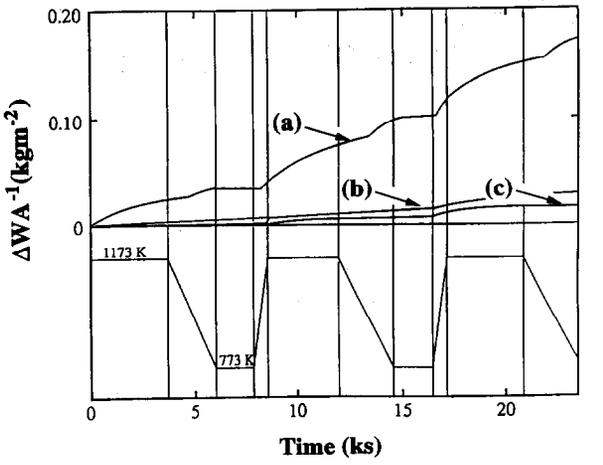

Fig. 10. Relationship between time and weight gain by the corrosion under the cyclic test between 1173 K to 773 K at P_{Br_2} = 4·4 kPa and P_{O_2} = 46 kPa. (a) TiC-coated SUS304; (b) TiC/SiC–20 mol% TiC double-layer-coated SUS304; (c) SiC/TiC FGM-coated SUS304.

Figure 10 shows the relationship between time and weight gain by the corrosion under the cyclic test between 1173 and 773 K at P_{Br_2} = 4·4 kPa and P_{O_2} = 46 kPa. TiC-coated SUS304 has less corrosion resistance. Both TiC/SiC-20 mol% TiC double-layer-coated SUS304, and the SiC/TiC FGM-coated SUS304 were covered with SiC on the surface.

Cracks in the film could not be avoided in the SiC/TiC double-layer-coated SUS304. However, the SiC/TiC FGM-coated SUS304 had no cracks (Figs 3 and 4). The result of corrosion experiments in the heat cyclic condition shows the capability of FGM coating to achieve thermal stress relaxation and corrosion resistance.

(b) m- and c-HfO_2 films

Figure 11 shows the weight change of the HfO_2-coated-SUS304 under the isothermal corrosion experiments at a T_{cor} of 1173 K, a P_{Br_2} of 4·4 kPa, a P_{O_2} of 46 kPa, a P_{tot} of 0·1 MPa, and at *a* t_{cor} of 21·6 ks. The specimens used for the corrosion experiments were the columnar m-HfO_2 with film thickness of 14 and 4 μm, the plate-like m-HfO_2 with thickness of 4 μm, the columnar c-HfO_2 with thickness of 14 μm, and bare SUS304. c-HfO_2-coated SUS304 was not corrosion resistant, while m-HfO_2-coated SUS304 showed a superior corrosion resistance.

XRD measurements of bare SUS304 and c-HfO_2-coated SUS304 showed that after the corrosion experiments, Fe_2O_3, Fe_3O_4 and Cr_2O_3 were formed. On the surface of the specimens after the corrosion experiments, the detachment of oxide scale from the SUS304, with a thickness of 0·19 μm could be observed. In the case of c-HfO_2-coated SUS304, the detachment of the film from

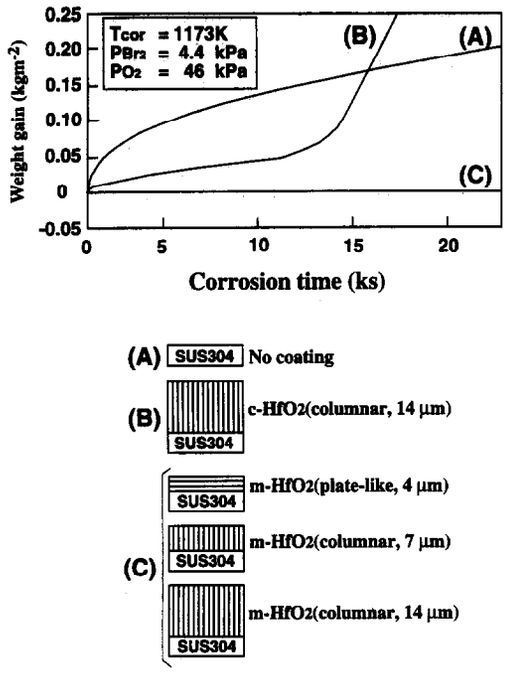

Fig. 11. Relationship between time and weight gain of m-HfO_2-coated SUS304 by the corrosion at T_{cor} = 1173 K, P_{Br_2} = 4·4 kPa and P_{O_2} = 46 kPa (isothermal condition).

the SUS304 partially occurred. The corrosion and the detachment of the film might occur around the interface of c-HfO_2 film and SUS304.

The corrosion resistance of the m-HfO_2-coated SUS304, which revealed the superior corrosion resistance under isothermal conditions, was investigated by the heat-cyclic corrosive test.

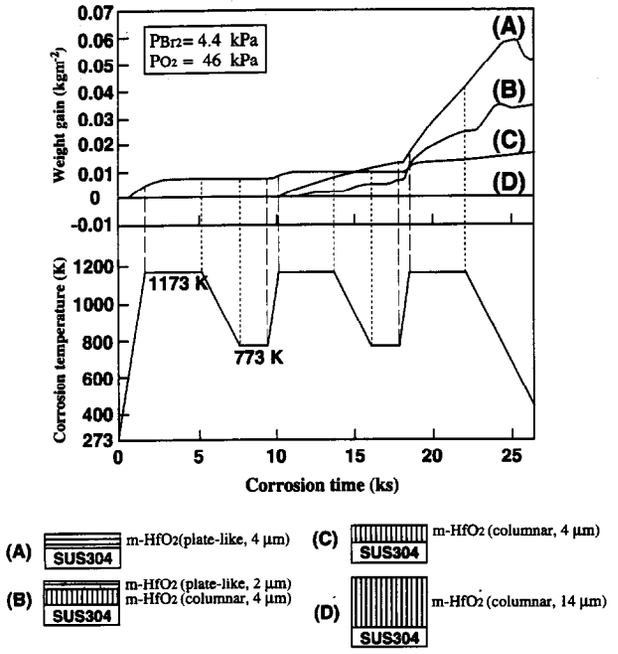

Fig. 12. Relationship between time and weight gain by the corrosion under the cyclic test between 1173 K to 773 K at P_{Br_2} = 4·4 kPa and P_{O_2} = 46 kPa. (a) m-HfO_2 (plate-like, 4 μm); (b) m-HfO_2 (columnar, 4 μm; plate-like, 2 μm); (c) m-HfO_2 (columnar, 4 μm); (d) m-HfO_2 (columnar, 14 μm).

Figure 12 shows the temperature change and the experimental results of the weight change of m-HfO_2-coated SUS304. The columnar m-HfO_2 (14 μm) coated SUS304 had superior corrosion resistance. Corrosion resistance decreased in the order: columnar m-HfO_2(4 μm), m-HfO_2 (texture changed from columnar to plate-like), plate-like m-HfO_2.

The examination of the surfaces of plate-like m-HfO_2 (4 μm in thickness) and columnar m-HfO_2 (14 μm in thickness) by SEM after the cyclic heating corrosion test, showed that the excellent corrosion resistance of the 14 μm-columnar m-HfO_2 coated SUS304, was related to the absence of cracks and detachment from the substrate. This is thought to be due to the effects of columnar texture on the thermal stress relaxation, and of the excellent corrosion resistance of the m-HfO_2.

4 Conclusions

Coatings of TiC, SiC–TiC, SiC/TiC FGM, m-HfO_2 and c-HfO_2 on stainless steel (SUS304) using CVD method were examined as possible corrosion resistant structural materials for 'UT-3.' The corrosion resistance of these materials in a Br_2–O_2–Ar corrosive atmosphere was investigated. The following results were obtained:

Changing the source gas concentration leads to composition control in the TiC–SiC composite films. The composition of TiC–SiC films prepared at a deposition temperature of 1323 K and at a total gas pressure of 0·1 MPa agreed with calculations. The SiC–20 mol% TiC composite film was prepared at a MTS/($TiCl_4$ + MTS) of 0·7. Cracks in the films after CVD could not be avoided in either the TiC-coated or the SiC, TiC double-layer-coated SUS304. However, both the TiC and SiC–20 mol% TiC double-layer-coated SUS304, and the SiC/TiC FGM-coated SUS304 had no cracks. Corrosion of the TiC and SiC–20 mol% TiC double-layer-coated SUS304 was mainly caused by oxidation of the TiC film and SUS304. SiC/TiC FGM-coated SUS304 showed superior corrosion resistance in isothermal and cyclic heating conditions.

Cracks in the m- and c-HfO_2 films after CVD could not be avoided in neither plate-like m-HfO_2 nor plate-like c-HfO_2. Columnar m-HfO_2-coated or columnar c-HfO_2-coated SUS304 had no cracks. Corrosion of the c-HfO_2-coated or plate-like-m-HfO_2-coated SUS304 was mainly caused by oxidation of the SUS304. Columnar m-HfO_2-coated SUS304 showed superior corrosion resistance in isothermal and cyclic heating conditions. This is

thought to be due to the effects of columnar texture on the thermal stress relaxation, and of the excellent corrosion resistance of the m-HfO_2.

Acknowledgement

This research was partially supported by a Grant-in-Aid for Scientific Research from the Ministry of Education, Science and Culture.

References

1. Sasaki, M., Hiratani, T. & Hirai, T., Corrosion Resistance of SiC/TiC FGM-coated Stainless Steel in Br_2–O_2–Ar Atmosphere, *Proc. 2nd Int. Symp. Functionally Gradient Materials*, 1993, pp. 369–376.
2. Niino, M., Hirai, T. & Watanabe, R., Functionally Gradient Materials as Heat-resistant Use for Space Plane, *J. Japan Soc. Composite Materials, (in Japanese)*, **13** (1987) 257–264.
3. Sasaki, M., Wang, Y., Hirano, T. & Hirai, T., Design of SiC/C Functionally Gradient Material and Its Preparation by Chemical Vapor Deposition, *J. Ceram. Soc. Jpn. Inter. Ed.*, **97** (1989) 530–534.
4. Kumakawa, A., Maeda, S., Sasaki, M., Niino, M., Sakamoto, A., Sasaki, M. & Hirai, T., Evaluation of Thermomechanical Properties of Functionally Gradient Material under High Temperature Difference, *Proc. European Space Agency Symp.*, ESA SP-303, 1990, pp. 339–344.
5. Sasaki, M. & Hirai, T., Fabrication and Thermal Barrier Characteristics of CVD SiC/C Functionally Gradient Material, Proc. *1st Int. Symp. Functionally Gradient Material*, edited by M. Yamanouchi, M. Koizumi, T. Hirai and I. Shiota, 1990, pp. 83–88.
6. Sasaki, M. & Hirai, T., Fabrication and Evaluation of SiC/C Functionally Gradient Material, *Journal de Physique IV*, **C2** (1991) 649–655.
7. Sasaki, M. & Hirai, T., Fabrication and Properties of Functionally Gradient Materials. The Centennial Memorial Issue of The Ceramic Society of Japan, *J. Ceramic Soc. Jpn.*, **99** (1991) 1002–1013.
8. JANAF Thermochemical Tables, 2nd Ed. No.NRSDS-NBS-37, edited by D. R. Stull and H. Prophet, U.S. Government Printing Office, Washington DC, 1971.